Research Square

Preprints are preliminary reports that have not undergone peer review.
They should not be considered conclusive, used to inform clinical practice,
or referenced by the media as validated information.

A Calculation Model for the Loess Collapse Coefficient Considering Progressive Wetting, Dry Density, and Applied Vertical Pressure Calculation Model for Moisture-Induced Collapse of Loess Considering Three Factors: Overburden Pressure, Water Content and Density

Aijun ZHANG

zaj@nwsuaf.edu.cn

Xijing University

Jianguo DU

Xijing University

Zhichao LIANG

Shangluo University

Article

Keywords: wetting-induced collapse, collapse coefficient, three-factor coupled model, degree of saturation, void ratio

Posted Date: September 18th, 2026

DOI: https://doi.org/10.21203/rs.3.rs-10862154/v1

License: This work is licensed under a Creative Commons Attribution 4.0 International License.
Read Full License

Additional Declarations: No competing interests reported.

Version of Record: A version of this preprint was published at Scientific Reports on October 16th, 2026. See the published version at https://doi.org/10.1038/s41598-026-75714-7.

Article

A Calculation Model for the Loess Collapse Coefficient Considering Progressive Wetting, Dry Density, and Applied Vertical Pressure

Calculation Model for Moisture-Induced Collapse of Loess Considering Three Factors: Overburden Pressure, Water Content and Density

Aijun ZHANG[1,2,3]*, Jianguo DU [1,2] and Zhichao LIANG [3,4]

1 School of Civil Engineering ,Xijing University, Xian 710123, China; zaj@nwsuaf.edu.cn (A.ZHANG) 1309058975@qq.com(J.DU), 13186055201@163.com(Z.LIANG)
2 Shaanxi Key Laboratory of Safety and Durability of Concrete Structures, Xi'an 710123, China
3. School of Water Resources and Civil Engineering, Northwest A&F University, Yangling 712100, China;
4 School of Urban and Rural Planning and Architectural Engineering, Shangluo University, Shangluo 726000, China;
* Correspondence: zaj@nwsuaf.edu.cn; Tel.: 139 9184 3800

Abstract

To quantify the coupled effects of moisture state, pore-structure state, and applied vertical pressure on loess collapsibility, a series of laboratory collapse tests was conducted on remolded loess collected from the Ili region of Xinjiang, China. The water content ranged from 6.6% to 21.0%, the dry density ranged from 1.24 to 1.47 g/cm^3, and the applied vertical pressure ranged from 50 to 2000 kPa. The relationships of the collapse coefficient with water content, degree of saturation, dry density, and applied vertical pressure were first examined. Dry density was converted to void ratio, while degree of saturation was calculated from water content and void ratio. Based on the observed nonlinear pressure response, a pressure-dependent formulation with fixed exponents m=1.6 and n=1.0 was adopted. The model parameters were further expressed as continuous functions of degree of saturation and void ratio, yielding a three-factor coupled model governed by dimensionless pressure, degree of saturation, and void ratio.

Model performance was evaluated using all valid test data and by comparing calculated response surfaces with measured results under different void-ratio conditions. The collapse coefficient generally decreased with increasing water content and degree of saturation, while the influence of pore-structure state depended on both moisture state and applied vertical pressure. The pressure-dependent response was distinctly nonlinear, typically increasing to a peak and then decreasing or approaching a relatively stable value. Back-calculation of the complete model yielded R^2=0.783, RMSE = 0.0217, and MAE = 0.0171, indicating that the model satisfactorily captured the principal variations in collapse coefficient within the investigated range.

A wetting parameter was further introduced to characterize the relative progression from the initial moisture state toward theoretical saturation. Within the experimentally investigated range, the wetting parameter varied from 0 to 0.5839, corresponding to degrees of saturation from 0.1504 to 0.6717. The measured normalized proportions of the interval-

averaged collapse coefficients across four saturation intervals were 39.16%, 23.83%, 19.38%, and 17.63%, while the corresponding calculated values were 37.82%, 26.80%, 21.05%, and 14.34%, respectively. The comparison indicates that the model reasonably reproduces the overall reduction in collapse response with increasing degree of saturation, although it slightly underestimates the response at relatively high saturation levels.

The engineering applicability of the proposed model was further examined using a 30 m large-scale field immersion test reported for the Ili region. The model-predicted self-weight collapse was 3330.71 mm, compared with the measured value of 3520 mm, corresponding to a relative error of 5.38%. These results show that the proposed model provides a practical framework for evaluating loess collapsibility and estimating foundation self-weight collapse from depth-dependent moisture and density data within the investigated stress and state ranges.

Keywords: wetting-induced collapse; collapse coefficient; three-factor coupled model; degree of saturation; void ratio

1. Introduction

Loess is an aeolian silt deposit formed during the Quaternary under arid and semi-arid climatic conditions [1]. It is typically yellow to yellowish brown and commonly exhibits a metastable, open-pore structure in its natural unsaturated state. In China, loess is widely distributed across the northern and northwestern regions, including Xinjiang, and covers approximately 6.35×105km^2, accounting for about 6.6% of the national land area [2-4]. Its high void ratio, low natural density, and weak interparticle bonding make it particularly susceptible to wetting-induced structural collapse [5-11]. When wetting occurs under load, interparticle bonds weaken and the metastable structure undergoes rapid rearrangement [12], producing additional settlement beyond conventional compression. Such deformation may compromise the serviceability and safety of engineering structures, making loess collapsibility a major concern in geotechnical engineering.

Wetting-induced collapse also plays an important role in loess landform evolution, geological hazard development, and infrastructure damage. The associated risks are particularly significant in reservoirs, canals, slopes, pavements, and foundation systems, where rainfall infiltration, reservoir impoundment, and groundwater-level fluctuations continuously alter the soil moisture state. Progressive wetting weakens the original soil fabric and reduces structural stability, potentially leading to landslides, slope failure, pavement subsidence, and differential settlement of buildings [3].

In water conservancy and hydraulic engineering projects, variations in the soil moisture state caused by reservoir impoundment, seepage infiltration, and groundwater-level fluctuations can alter matric suction and interparticle bonding. Under existing stress conditions, progressive wetting may degrade the metastable loess structure, resulting in additional settlement and deformation.

Such wetting-induced deformation is particularly concerning for hydraulic structures constructed in loess regions, including reservoirs, water conveyance facilities, and pumped-storage hydropower stations. Long-term changes in the surrounding moisture state may increase the risk of foundation settlement, differential deformation, and slope instability. Liu et al. [28] demonstrated that water infiltration significantly affects the mechanical response of collapsible loess and alters the load-transfer behavior of engineering structures. Therefore, developing a quantitative model for evaluating loess collapsibility

under different stress levels, moisture states, and pore-structure conditions is important for the design and performance assessment of hydraulic engineering projects.

Previous studies have examined loess collapsibility in relation to moisture condition, dry density, stress level, stress path, water infiltration, and structural degradation. Wetting-induced collapse is generally attributed to the breakdown of the metastable soil fabric and the subsequent rearrangement of particles under load [12]. Experimental evidence indicates that initial water content, dry density, stress level, and stress path jointly affect the magnitude and development of collapse deformation, whereas increased compaction generally reduces collapse potential [13,14]. Field and laboratory studies have further shown that sustained infiltration promotes structural weakening and additional settlement, while the resulting deformation response depends on the interaction between moisture migration and the prevailing stress state [15-17]. These findings demonstrate that loess collapsibility is governed by interacting stress and state variables rather than by a single factor.

Recent advances in imaging and microstructural characterization have improved the understanding of the mechanisms underlying wetting-induced collapse. Existing observations indicate that changes in pore-size distribution, particle arrangement, interparticle bonding, and macropore connectivity are closely associated with the macroscopic deformation of loess during wetting [18-20]. For lime-treated Ili loess, Liang et al. [21] found that curing-induced changes in microstructure were accompanied by marked variations in water-retention behavior, further demonstrating the close coupling between pore structure and moisture state. These studies provide an important basis for interpreting loess collapsibility from both macroscopic and microstructural perspectives.

Nevertheless, several research gaps remain. First, most existing studies have examined the effects of moisture state, dry density, stress path, and pore structure separately, whereas the coupled response of loess collapsibility to simultaneous variations in applied stress, moisture state, and pore-structure state has not been fully quantified. Second, conventional collapse tests generally represent discrete initial states, while loess in engineering practice is often subjected to progressive wetting caused by rainfall infiltration, groundwater-level fluctuations, or reservoir impoundment. The evolution of collapse potential during such wetting processes remains insufficiently understood. Third, a continuous formulation that relates the collapse coefficient to applied stress level, moisture state, and pore-structure state is still required for practical evaluation under changing soil conditions.

Accordingly, this study investigated the collapsibility of remolded Ili loess under different water-content conditions, dry densities, and applied vertical pressures using the double-oedometer method. The effects of moisture state, dry-density condition, and applied vertical pressure on the collapse coefficient were first examined. The dry density was subsequently converted to void ratio, while the degree of saturation was calculated from the water content and void ratio, and a three-factor coupled model was developed in terms of dimensionless pressure, degree of saturation, and void ratio. A wetting parameter was further introduced to describe the progression of wetting within the experimentally investigated range. The proposed framework provides a continuous means of evaluating the collapse coefficient of Ili loess under varying applied vertical pressure, moisture state, and pore-structure state.

2.Materials and Methods

2.1 Materials

The soil used in this study was collected from the fourth terrace on the left bank of the Tekes River in Ili, Xinjiang, China, at depths of 8.0–15.0 m. The soil samples were collected during the site investigation for a proposed hydropower project in Ili, Xinjiang, China, and permission for field sampling was obtained from the local government prior to sample collection. The sampled loess was yellow in color. To reduce the influence of spatial heterogeneity within the deposit, bulk soil was manually collected from several locations across the sampling area. Field observations showed only minor variations in particle-size composition with depth, indicating that the soil layer was relatively uniform.

The particle-size distribution was determined by laser diffraction using an LS 13 320 particle size analyzer, whereas the specific gravity and Atterberg limits were measured in accordance with GB/T 50123-2019 [23]. The soil comprised approximately 0.5% sand, 81.5% silt, and 18.0% clay, accounting for 100% of the sample. The colloidal fraction represented 10.1% of the total soil mass and was included within the clay fraction rather than treated as a separate particle-size component. The specific gravity of the soil solids was 2.72, while the plastic limit, liquid limit, and plasticity index were 17.0%, 28.0%, and 11, respectively. According to the Unified Soil Classification System, the soil was classified as low-plasticity clay (CL). The basic physical properties of the tested soil are summarized in Table 1.

Table 1. Basic physical properties of the tested loess.

Sampling depth H	Specific gravity G_S	Plastic limit w_P	Liquid limit w_L	Plasticity index I_P	Sand	Silt	Clay	Soil classification
m	—	%	%	%	%	%	%	—
8.0-15.0	2.72	17.0	28.0	11.0	0.5	81.5	18.0	CL

2.2 Experimental Program

To investigate the effects of water content and dry density on loess collapsibility, collapse tests were conducted on specimens prepared under five water-content conditions and four target dry densities. The tested water contents were 6.6%, 12.5%, 14.1%, 18.2%, and 21.0%, while the corresponding target dry densities were 1.24, 1.31, 1.39, and 1.47 g/cm^3. These conditions enabled a systematic evaluation of the effects of moisture state and pore-structure state on the collapse behavior of loess.

In accordance with the Standard for Building Construction in Collapsible Loess Regions (GB 50025-2018) [24] and the requirements of laboratory oedometer testing, seven applied vertical pressures were used: 50, 100, 200, 400, 800, 1200, and 2000 kPa. The maximum applied vertical pressure was 2000 kPa to characterize the collapse response over a broad pressure range.

2.3 Specimen Preparation and State-Variable Definition

Before specimen preparation, the collected loess was oven-dried at 105 °C, gently disaggregated, and passed through a 2 mm sieve. The required amount of water was then added uniformly using a fine-spray method to achieve the prescribed water content. The moistened soil was sealed with plastic film and allowed to equilibrate for 24 h to ensure uniform moisture distribution.

The specimens were subsequently prepared by layered static compaction. The thoroughly mixed soil was placed into a standard cutting ring with an inner diameter of 61.8 mm and a height of 20 mm. The mass of soil added to each layer and the degree of compaction were carefully controlled to achieve the prescribed dry density. After preparation,

the mass and dimensions of each specimen were measured to confirm that the target testing conditions had been satisfied. All specimens were prepared using the same procedure to ensure consistency among the tests.

To facilitate comparison among specimens with different soil-state conditions, the measured pressure, water content, and dry density were expressed using representative state variables before analysis. The applied vertical pressure was normalized by the reference atmospheric pressure to obtain the dimensionless pressure P. The dry density was converted to void ratio e, while the degree of saturation S_r was calculated from the water content and void ratio, as follows:

$$P = \frac{p}{p_a} \quad (1)$$

$$e = \frac{G_s \rho_w}{\rho_d} - 1 \quad (2)$$

$$S_r = \frac{wG_s}{e} \quad (3)$$

The variables P, S_r, and e were subsequently used to represent the applied vertical pressure level, moisture state, and pore-structure state, respectively.

2.4 Collapse Test Procedure

Laboratory collapse tests were conducted to evaluate the collapsibility of loess under different water-content and dry-density conditions. The double-oedometer method was adopted for the main test program, while selected single-oedometer tests were conducted as supplementary verification. All tests followed the procedures and deformation-stability criteria specified in the Standard for Geotechnical Testing Method (GB/T 50123–2019) [23].

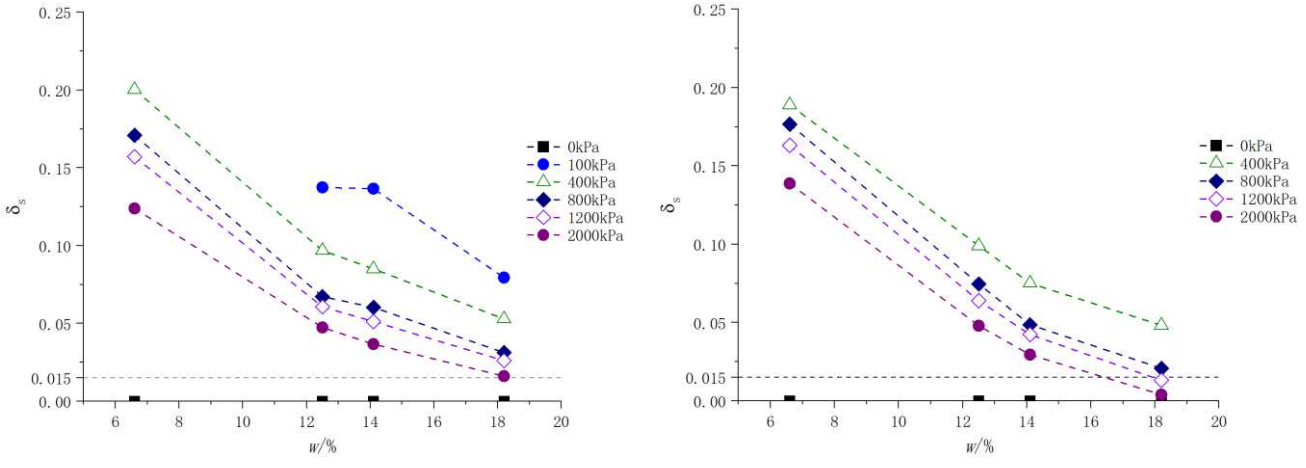
According to the Standard for Building Construction in Collapsible Loess Regions (GB 50025–2018) [24], the collapse coefficient is defined as follows:

$$\delta_s = \frac{h_p - h_p'}{h_0} \quad (4)$$

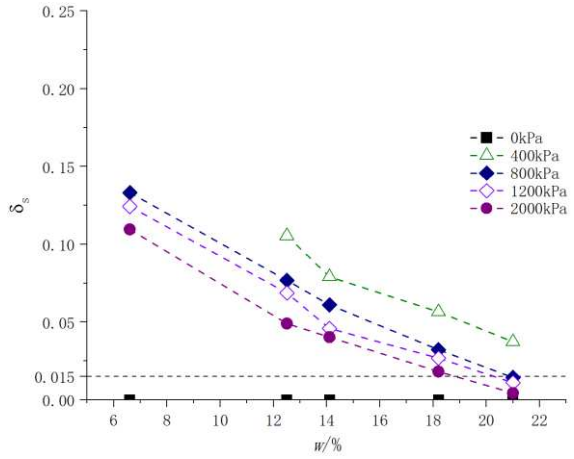
where δ_s is the collapse coefficient; h_p is the stabilized specimen height under a specified vertical pressure before inundation, mm; h_p' is the stabilized specimen height under the same vertical pressure after inundation and saturation, mm; and h_0 is the initial specimen height, mm.

3. Results and Discussion

3.1 Relationships of the collapse coefficient with water content and degree of saturation



(**a**) (**b**)



(**c**)

Figure 1. Relationships between the collapse coefficient and water content under different dry-density conditions: (**a**) ρ_d=1.24g/cm^3; (**b**) ρ_d=1.31g/cm^3; (**c**) ρ_d=1.39g/cm^3.

Figures 1(a)-(c) show that the collapse coefficient generally decreased with increasing water content under all investigated dry-density conditions. The decrease was particularly pronounced as the water content increased from 6.6% to approximately 12.5%–14.1%, whereas the curves gradually flattened at higher water contents of 18.2%–21.0%. These results indicate that loess collapsibility is more sensitive to changes in moisture state at relatively low water contents, whereas the remaining collapse potential gradually decreases as the soil approaches a wetter state.

The observed trend can be attributed to the influence of moisture state on the wetting-induced structural response of loess. At relatively low water contents, the specimens retained greater potential for structural rearrangement upon inundation, resulting in relatively large collapse deformation. As the water content increased, the difference between the soil states before and after inundation decreased, thereby reducing the additional deformation induced by wetting. The collapse response was also affected by dry density and applied vertical pressure. Specimens with lower dry densities generally exhibited larger collapse coefficients, while the differences among the pressure-dependent curves indicate that the effect of water content on collapsibility was also dependent on the applied pressure.

Overall, increasing water content reduced the measured collapse coefficient and caused several curves to approach or fall below the collapsibility criterion of δ_s=0.015. However, water content alone does not fully characterize the actual moisture state because the same water content may correspond to different degrees of pore-water filling under different pore-structure states. Previous research on Ili loess has also shown that soluble salt content can affect unfrozen-water content and matric suction under cooling conditions [22], further indicating that the internal water state of loess may be influenced by both pore structure and physicochemical conditions. Therefore, the degree of saturation was adopted as a more representative indicator of moisture state, and its relationship with the collapse coefficient was further examined.

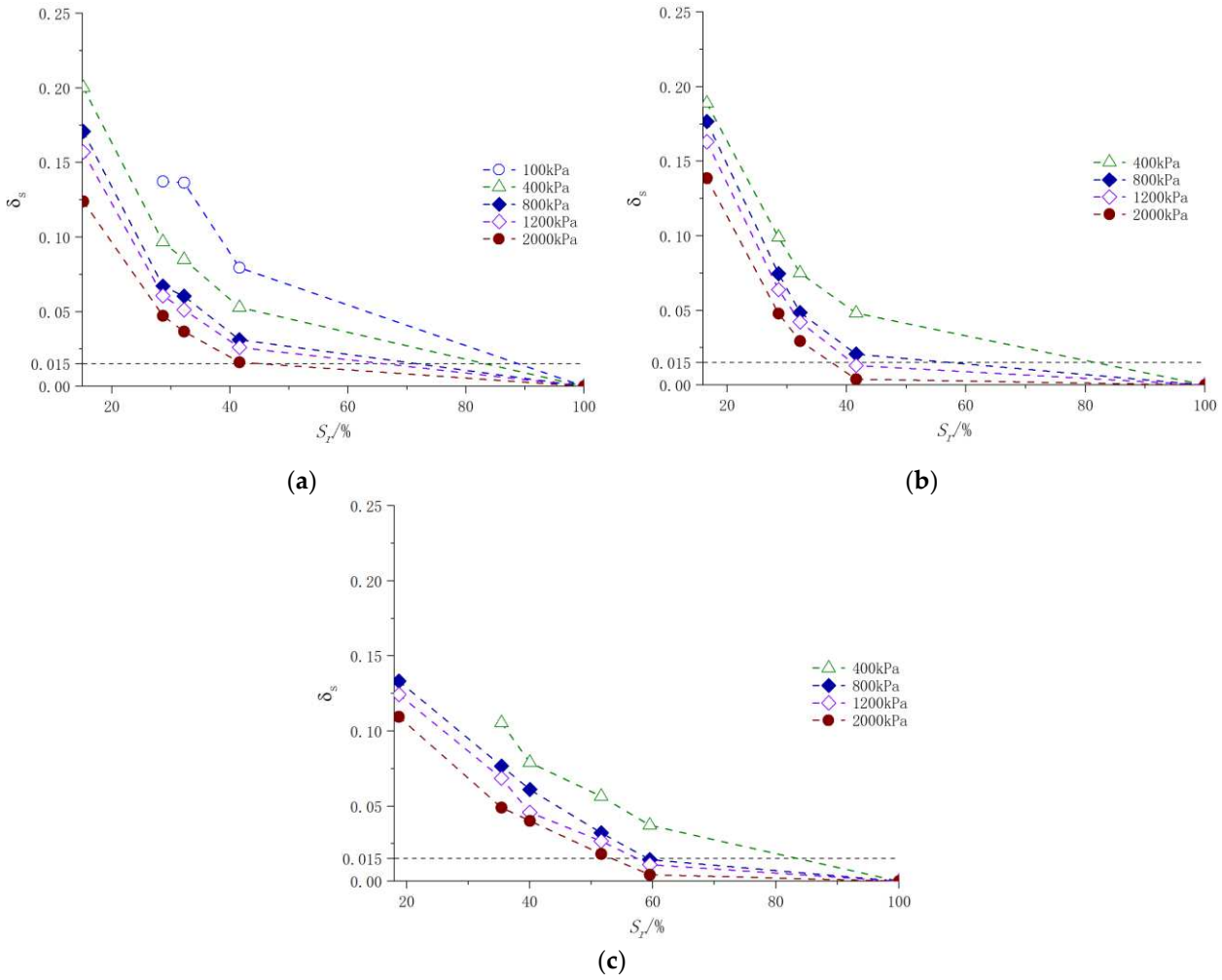


Figure 2. Relationships between the collapse coefficient and degree of saturation under different applied vertical pressures: (**a**) ρ_d=1.24g/cm^3; (**b**) ρ_d=1.31g/cm^3; (**c**) ρ_d=1.39g/cm^3.

Figures 2(a)-(c) illustrate the relationship between the collapse coefficient and degree of saturation under different dry-density conditions. Compared with water content, degree of saturation provides a more direct measure of the extent to which the pore space is occupied by water. The collapse coefficient generally decreased with increasing degree of saturation. At relatively low degrees of saturation, the curves decreased rapidly, indicating that loess collapsibility was highly sensitive to changes in moisture state. As the degree of saturation increased beyond approximately 50%, the collapse coefficient continued to decrease, although the rate of reduction became smaller. Within the investigated saturation range, the curves gradually approached relatively low values, indicating a progressive reduction in the remaining collapse potential.

Overall, increasing degree of saturation was associated with a reduction in the collapse coefficient. However, water content alone cannot fully characterize the moisture state of the specimens because soils with different dry densities may exhibit different degrees of pore-water filling at the same water content. Therefore, in the subsequent model development, dry density was converted to void ratio, while degree of saturation was calculated from water content and void ratio. The degree of saturation and void ratio, together with the dimensionless pressure P, were then incorporated into the coupled collapse-coefficient model.

3.2 Relationship between the Collapse Coefficient and Void Ratio

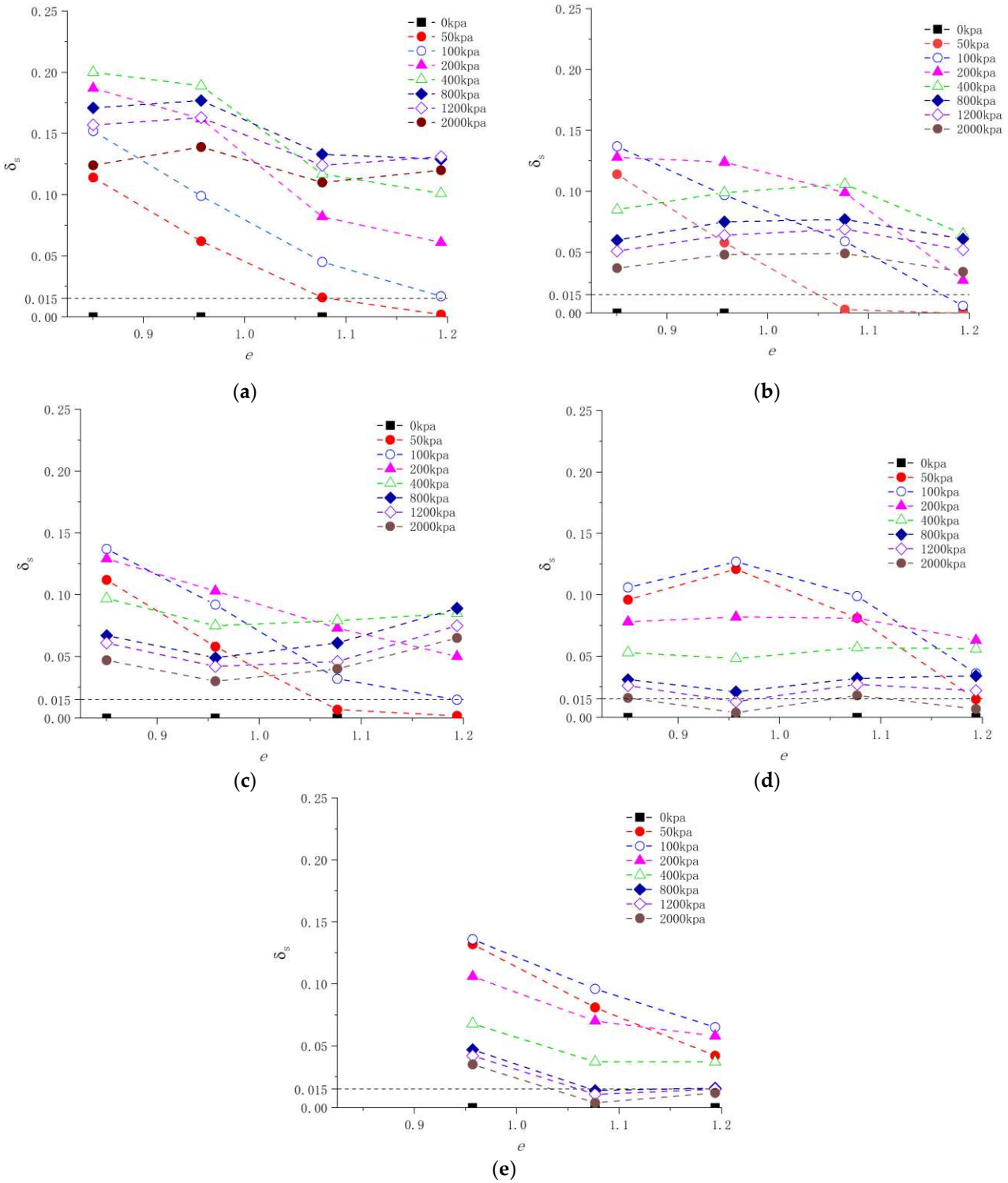


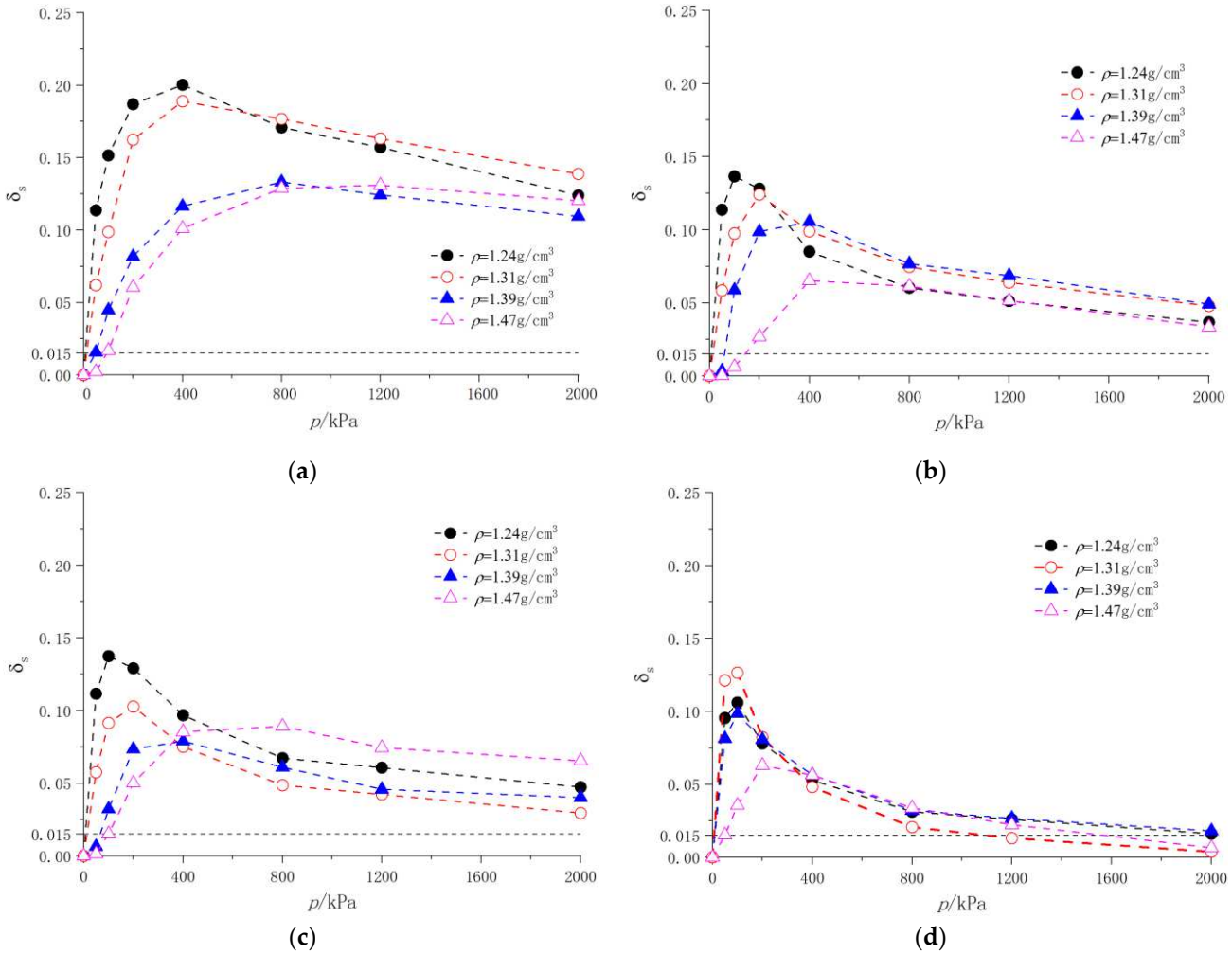
Figure 3. Relationships between the collapse coefficient and void ratio under different water-content conditions: (**a**) w=6.6%; (**b**) w=12.5%; (**c**) w=14.1%; (**d**) w=18.2%; (**e**) w=21%.

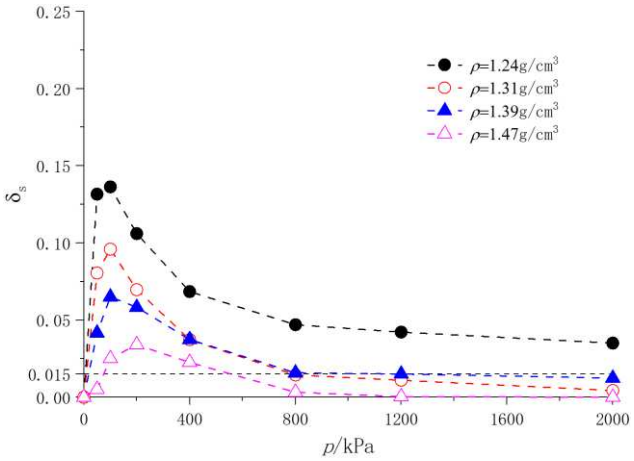
Figures 3(a)–(e) illustrate the relationships between the collapse coefficient and void ratio under different water-content conditions. The influence of void ratio on the collapse coefficient varied with both water content and applied vertical pressure. Under several pressure conditions, noticeable differences in the collapse coefficient were observed among specimens with different void ratios, whereas non-monotonic variations occurred under some combinations of water content and pressure. These results indicate that the effect of pore-structure state on loess collapsibility cannot be considered independently of moisture state and applied vertical pressure.

Because void ratio is inversely related to dry density, changes in *e* reflect variations in the pore-structure state of the specimens. However, the influence of pore structure on the collapse response depended strongly on the water-content condition. At relatively low water contents, differences among the void-ratio conditions were generally more pronounced, whereas these differences tended to decrease as the soil approached a wetter state. This behavior indicates a coupled influence of moisture state and pore-structure state on the wetting-induced collapse response.

Differences were also observed among the curves corresponding to different applied vertical pressures. The magnitude and variation of the collapse coefficient with void ratio changed with pressure, indicating that applied vertical pressure modified the contribution of pore-structure state to the collapse response. Therefore, neither void ratio nor moisture state alone can fully characterize loess collapsibility. The coupled effects of dimensionless pressure, degree of saturation, and void ratio were consequently incorporated into the subsequent collapse-coefficient model.

3.3 Relationship between the Collapse Coefficient and Applied Vertical Pressure





(**e**)

Figure 4. Relationships between the collapse coefficient and applied vertical pressure under different water-content conditions: (**a**) w=6.6%; (**b**) w=12.5%; (**c**) w=14.1%; (**d**) w=18.2%; (**e**) w=21%.

Figures 4(a)-(e) illustrate the relationship between the collapse coefficient and applied vertical pressure under different water-content conditions. The collapse coefficient did not vary monotonically with applied vertical pressure. Instead, it generally increased over the low-to-intermediate pressure range, reached a maximum within an intermediate pressure interval, and subsequently decreased or approached a relatively stable value. This behavior indicates the existence of a pressure-sensitive range in which wetting-induced collapse is more pronounced. Beyond this range, further increases in applied vertical pressure did not necessarily result in larger collapse coefficients.

The pressure corresponding to the maximum collapse coefficient varied among the different dry-density conditions. For several specimens, relatively large collapse coefficients occurred within the applied-pressure range of approximately 100–400 kPa, although the peak position differed among the individual soil states. This variation indicates that the pressure-dependent collapse response was influenced by the pore-structure state of the soil. In general, looser specimens exhibited greater susceptibility to wetting-induced structural rearrangement, whereas denser specimens showed different pressure-dependent response characteristics.

Under conditions of low water content or relatively low dry density, the collapse coefficient remained above the collapsibility criterion of δ_s=0.015 even at an applied vertical pressure of 2000 kPa, indicating that appreciable collapse potential persisted at high stress levels. By contrast, under conditions of higher water content or greater dry density, some curves approached or fell below δ_s=0.015 at pressures of approximately 800-1200 kPa. This result indicates that the collapse potential was substantially reduced and that some specimens could be classified as non-collapsible according to the adopted criterion.

Therefore, a single pressure threshold cannot be used to determine whether loess becomes non-collapsible, because the corresponding pressure depends on both moisture state and pore-structure state. Within the investigated range, the collapse coefficients of many wetter or denser specimens decreased to relatively low values at applied vertical pressures of 1200–2000 kPa. In contrast, some specimens at lower water contents retained appreciable collapse coefficients over the same pressure range, indicating that collapse potential may persist even under relatively high applied vertical pressures.

Overall, the collapse coefficient exhibited a nonlinear pressure-dependent response characterized by an initial increase followed by a subsequent decrease. Water content and dry density affected the magnitude and pressure-dependent evolution of the collapse re-

sponse. These results indicate that loess collapsibility is governed by the coupled influences of applied vertical pressure, moisture state, and pore-structure state. Accordingly, the subsequent model was formulated on the basis of the nonlinear pressure response and incorporated degree of saturation and void ratio to represent the combined influences of moisture state and pore-structure state. Sun et al. [25] similarly reported that the collapse coefficient is jointly controlled by pressure, moisture condition, and density state and that its variation with pressure is distinctly nonlinear.

4. Computational Model

4.1 Three-factor coupled model for the collapse coefficient

The results presented in Section 3 demonstrate that the collapse coefficient varied nonlinearly with applied vertical pressure. At relatively low pressures, only limited collapse deformation developed. As the applied pressure increased, the soil structure became increasingly susceptible to wetting-induced rearrangement, resulting in a marked increase in the collapse coefficient. At higher pressures, however, greater compression before inundation reduced the remaining collapsible pore space, and the collapse coefficient gradually decreased. On this basis, a pressure-dependent relationship for the collapse coefficient was first established.

Marei et al. [27] investigated the wetting-induced deformation of collapsible soils under different combinations of vertical stress and degree of saturation and established relationships describing collapse strain as a function of stress level and moisture state. Their results indicated that collapse deformation is jointly influenced by the applied stress at wetting and the degree of saturation, supporting the use of a continuous nonlinear formulation involving both stress and soil-state variables. Accordingly, the nonlinear model proposed by Wang et al. [26] was adopted as the mathematical basis of the present study.

The nonlinear model proposed by Wang et al. [26] was originally developed to describe nonlinear stress–strain responses and is expressed as:

$$q = (\sigma_1 - \sigma_3) = [(a\varepsilon_1^m - c)exp(-b\varepsilon_1^n) + c]p_a \quad (5)$$

where q is the deviatoric stress (kPa); σ_1 is the axial stress (kPa); σ_3 is the confining pressure (kPa); ε_1 is the axial strain, expressed as a percentage; p_a is the reference atmospheric pressure, taken as 101.3 kPa; and a, b, c, m, and n are dimensionless fitting parameters. The exponents m and n primarily control the growth and attenuation characteristics of the nonlinear stress–strain response, respectively.

To express the governing state variables in dimensionless form and facilitate comparison among specimens with different soil-state conditions, the applied vertical pressure was normalized to obtain the dimensionless pressure P, the dry density was converted to void ratio e, and the degree of saturation S_r was calculated from water content and void ratio. The definitions of P, e, and S_r are given in Eqs. (1)–(3).

By replacing the original pressure variable in the model proposed by Wang et al. [26] with the dimensionless pressure P, the pressure-dependent collapse-coefficient relationship can be written as

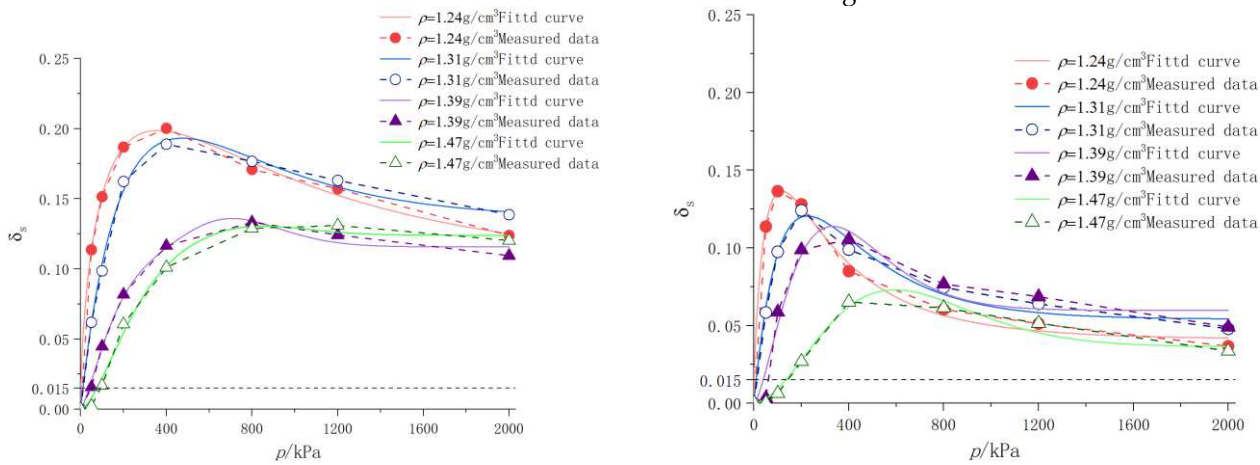
$$\delta_s = (aP^m - c)exp(-bP^n) + c \quad (6)$$

where δ_s is the dimensionless collapse coefficient, and a, b, c, m, and n are dimensionless fitting parameters. The fitted parameter values obtained from the experimental data are summarized in Table 2.

Table 2. Model parameters.

w/%	ρ_d/(g/cm^3)	S_r	a	b	c	m	n	R^2
6.6	1.24	0.15	0.347	1.550	0.101	1.300	0.482	0.991
6.6	1.31	0.167	0.082	0.551	0.136	1.236	0.828	0.992
6.6	1.39	0.188	0.025	0.253	0.107	1.258	1.040	0.995
6.6	1.47	0.211	0.008	0.136	0.123	1.607	1.414	0.991
12.5	1.24	0.285	1.000	2.323	0.042	1.267	0.521	0.989
12.5	1.31	0.316	0.206	1.261	0.054	1.508	0.725	0.961
12.5	1.39	0.355	0.046	0.437	0.060	1.773	1.184	0.951
12.5	1.47	0.4	0.006	0.148	0.036	2.163	1.407	0.976
14.1	1.24	0.321	1.000	2.419	0.050	1.320	0.504	0.993
14.1	1.31	0.356	0.466	2.056	0.035	1.802	0.623	0.981
14.1	1.39	0.401	0.030	0.402	0.043	1.765	1.153	0.957
14.1	1.47	0.451	0.011	0.151	0.066	1.783	1.405	0.992
18.2	1.24	0.415	0.467	2.276	0.032	2.056	3.467	0.992
18.2	1.31	0.46	1.000	2.182	0.007	0.882	0.518	0.992
18.2	1.39	0.517	1.000	2.578	0.020	1.243	0.485	0.992
18.2	1.47	0.582	1.000	3.376	0.003	2.484	0.452	0.976
21.0	1.31	0.531	1.000	2.305	0.038	1.001	0.541	0.998
21.0	1.39	0.597	1.000	2.461	0.008	1.311	0.566	0.995
21.0	1.47	0.672	1.000	2.995	0.013	2.047	0.575	0.991

The measured collapse coefficients and their corresponding fitted curves under different water-content conditions are shown in Fig. 7.



(**a**) (**b**)

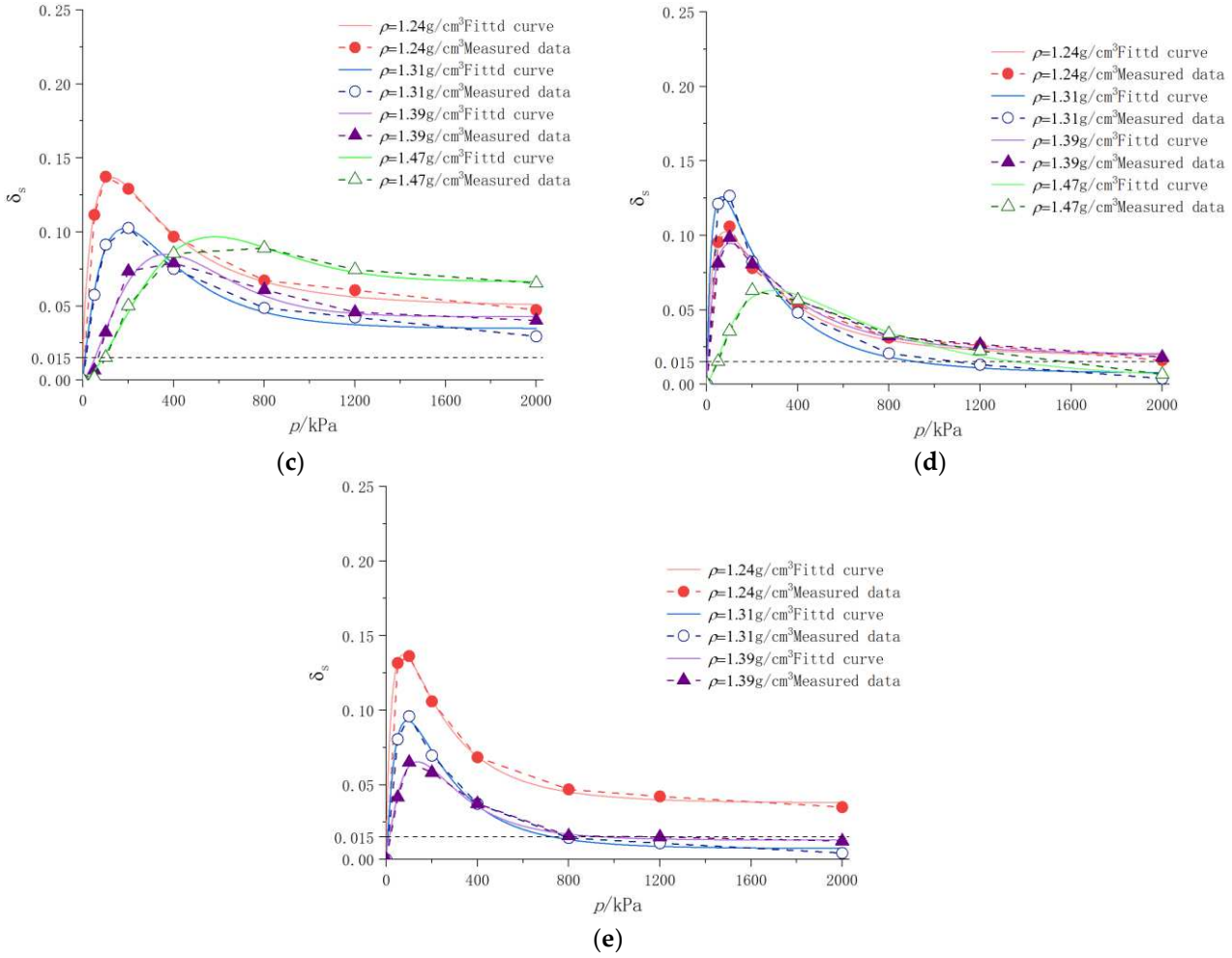


Figure 5. Comparison between the measured and fitted pressure-collapse coefficient curves at different water contents: (**a**) w=6.6%; (**b**) w=12.5%; (**c**) w=14.1%; (**d**) w=18.2%; (**e**) w=21%.

As shown in Figures 5(a)–(e), the fitted curves are generally consistent with the measured data and satisfactorily reproduce the overall variation in the collapse coefficient. At a given water content, variations in dry density affected both the peak collapse coefficient and the pressure corresponding to the peak. Specimens with lower dry densities generally possessed a looser pore structure and therefore exhibited greater collapse deformation upon inundation. As dry density increased, the soil structure became denser, the available collapsible pore space decreased, and the collapse coefficient generally declined. At a given dry density, increasing water content reduced the structural difference between the pre-inundation and post-inundation states, thereby decreasing the additional deformation induced by wetting and, consequently, the collapse coefficient.

Equation (6) captures the principal nonlinear variation of the collapse coefficient with pressure. As shown in Table 2, m controls the pressure-dependent growth of the power term, whereas n governs the attenuation behavior of the exponential term, thereby affecting the ascending and descending branches of the pressure–collapse coefficient curve. To reduce the number of model parameters while preserving its ability to describe the nonlinear pressure response, the fitted values of m and n obtained from all test groups using the original five-parameter model were statistically analyzed. The mean fitted values of m and n were 1.569 and 0.942, respectively. Accordingly, the exponents were fixed at m=1.6 and n=1.0 in the subsequent analysis.

The simplified model can therefore be expressed as follows:

$$\delta_s = (aP^{1.6} - c)exp(-bP) + c \quad (7)$$

The refitted parameters obtained from the experimental results are listed in Table 3.

Table 3. Refitted model parameters with fixed exponents m=1.6 and n=1.0.

w/%	ρ_d/(g/cm³)	S_r	a	b	c	R^2
6.6	1.24	0.15	0.161	0.952	0.153	0.627
6.6	1.31	0.167	0.0616	0.567	0.152	0.967
6.6	1.39	0.188	0.0169	0.336	0.108	0.995
6.6	1.47	0.211	0.00952	0.219	0.104	0.982
12.5	1.24	0.285	0.447	1.43	0.0542	0.895
12.5	1.31	0.316	0.153	0.904	0.0611	0.927
12.5	1.39	0.355	0.0532	0.509	0.0534	0.902
12.5	1.47	0.4	0.0129	0.254	0.0207	0.941
14.1	1.24	0.321	0.410	1.43	0.0639	0.868
14.1	1.31	0.356	0.182	1.01	0.0406	0.940
14.1	1.39	0.401	0.0356	0.472	0.0387	0.944
14.1	1.47	0.451	0.0146	0.289	0.0555	0.964
18.2	1.24	0.415	1.03	3.08	0.0304	0.856
18.2	1.31	0.46	0.759	1.84	0.0204	0.930
18.2	1.39	0.517	0.369	1.52	0.0306	0.897
18.2	1.47	0.582	0.0518	0.567	0.0137	0.944
21.0	1.31	0.531	0.710	1.87	0.0478	0.924
21.0	1.39	0.597	0.439	1.58	0.0143	0.947
21.0	1.47	0.672	0.176	1.20	0.0159	0.960

Table 3 indicates that, after fixing m=1.6 and n=1.0, the fitted parameters a, b, and c exhibited distinct variations with the degree of saturation, S_r. Parameters a and b generally increased with increasing S_r, although some fluctuations were observed under individual dry-density conditions. This indicates that the moisture state affects both the magnitude and attenuation characteristics of the pressure-dependent collapse response. In contrast, parameter c exhibited an overall decreasing tendency with increasing S_r, suggesting that the limiting component of the collapse response under high-pressure conditions generally decreased as wetting progressed.

The rates of variation in these parameters differed among the dry-density conditions, indicating that the pore-structure state influenced the relationship between degree of saturation and the pressure-dependent collapse response. Although some scatter was observed in individual test results, the fitted relationships captured the overall variations of the model parameters with Sr. These relationships therefore provided the basis for further establishing the dependence of the saturation-related fitting coefficients on the void ratio, e.

At a given dry density, the void ratio remains constant, whereas variations in water content are primarily reflected by changes in the degree of saturation. For each saturation state, a corresponding set of parameters a, b, and c was obtained by fitting the pressure–collapse coefficient relationship. Accordingly, under each fixed dry-density condition, Sr

was adopted as the primary state variable to characterize the moisture-dependent variation of the model parameters.

Because each dry-density (void-ratio) condition contained only four or five saturation states, the fitting relationships were restricted to simple functions containing no more than two adjustable coefficients to reduce the risk of overfitting. Based on the observed parameter trends, linear relationships were adopted for *a* and *b*, whereas *a* logarithmic relationship was adopted for *c*.

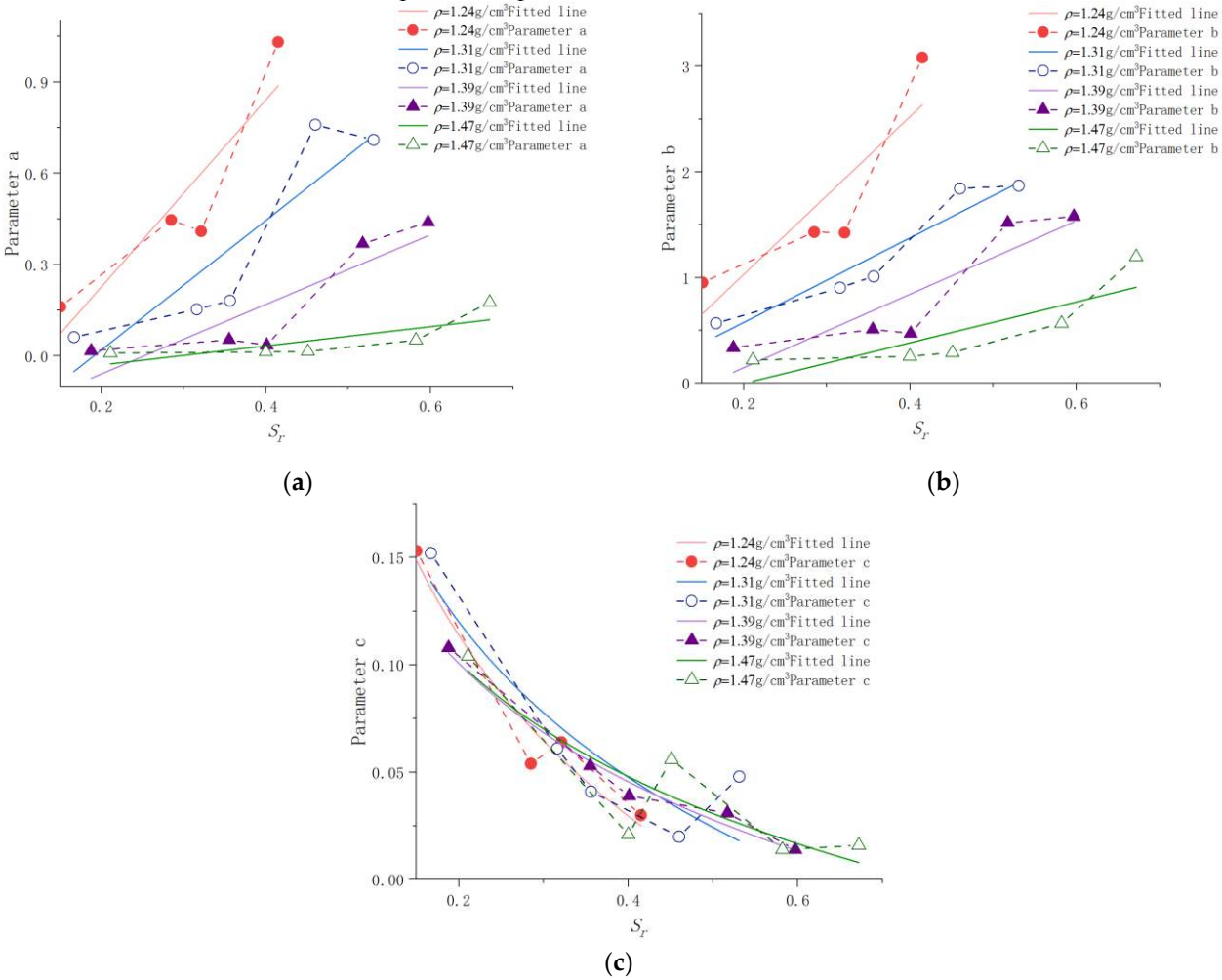


Figure 6. Relationships between the model parameters and degree of saturation under different dry-density conditions: (a) parameter *a*; (b) parameter *b*; and (c) parameter *c*. Symbols represent the fitted model parameters. Solid lines in (a) and (b) represent linear fitting relationships, whereas the solid curves in (c) represent logarithmic fitting relationships.

To quantify the parameter trends shown in Figure 6, the dependence of *a*, *b*, and *c* on the degree of saturation was described using the same functional forms under each fixed dry-density condition. The resulting relationships are expressed as follows:

$$a = A_a + B_a \cdot S_r \tag{8}$$

$$b = A_b + B_b \cdot S_r \tag{9}$$

$$c = A_c + B_c \cdot ln\left(S_r\right) \tag{10}$$

where A_a, B_a, A_b, B_b, A_c, and B_c are fitting coefficients that characterize the saturation-dependent relationships of the model parameters.

Table 4. Fitted relationships between the model parameters and degree of saturation.

ρ_d/(g/cm³)	Parameter	Relationship with degree of saturation S_r	R^2
1.24	a	$a=-0.386+3.07S_r$	0.838
1.24	b	$b=-0.464+7.47S_r$	0.770
1.24	c	$c=-0.0817-0.121\ln(S_r)$	0.956
1.31	a	$a=-0.407+2.14S_r$	0.800
1.31	b	$b=-0.228+4.01S_r$	0.911
1.31	c	$c=-0.048-0.104\ln(S_r)$	0.836
1.39	a	$a=-0.289+1.15S_r$	0.780
1.39	b	$b=-0.574+3.57S_r$	0.805
1.39	c	$c=-0.0722-0.0795\ln(S_r)$	0.984
1.47	a	$a=-0.0929+0.315S_r$	0.617
1.47	b	$b=-0.400+1.97S_r$	0.690
1.47	c	$c=-0.0226-0.077\ln(S_r)$	0.805

As shown in Table 4, under each fixed dry-density condition, parameters *a*, *b*, and *c* varied with the degree of saturation, although their rates of change and fitting performance differed among the parameter relationships. The fitted relationships for parameters *a* and *b* generally exhibited positive slopes, indicating an overall increase in both parameters with increasing S_r. These trends suggest that the moisture state affects both the magnitude and the pressure-dependent evolution of the collapse response.In contrast, parameter *c* decreased with increasing S_r, indicating that the limiting collapse coefficient under high-pressure conditions tended to decrease as the soil approached a wetter state.

The relationships between the model parameters and degree of saturation varied among the different dry-density groups. Parameters *b* and *c* generally showed moderate to good correlations with S_r, whereas parameter *a* exhibited greater scatter under some dry-density conditions. For example, at a dry density of 1.47 g/cm³, the coefficient of determination for the $a-Sr$ relationship was 0.617, which was lower than those obtained for the corresponding $b-S_r$ and $c-S_r$ relationships. This relatively weak correlation may be partly attributed to the limited number of saturation states and the small magnitude of parameter *a* under dense conditions. In addition, parameters *a*, *b,* and *c* jointly determine the pressure-dependent collapse response, and their effects on the calculated collapse coefficient are therefore coupled rather than independent. Consequently, the fitting performance of an individual parameter relationship does not necessarily translate directly into the predictive accuracy of the complete coupled model. Therefore, the R^2 values listed in Table 4 are used only to characterize the fitting performance of the individual parameter relationships, whereas the overall predictive accuracy of the coupled model is evaluated separately through back-calculation of the collapse coefficient.

At a given dry density, the void ratio remains constant, whereas variations in S_r represent changes in the moisture state of the specimen. Table 4 presents the relationships between parameters *a*, *b*, and *c* and S_r under the four investigated dry-density conditions. The coefficients A_a, B_a, A_b, B_b, A_c, and B_c obtained from these relationships provide discrete descriptions of the saturation-dependent parameter variation at the corresponding void-ratio levels. To incorporate the effect of pore-structure state into a unified formulation, the variation trends of these coefficients with void ratio were further considered.

The void ratios corresponding to the four dry densities were 1.194, 1.076, 0.957, and 0.850. The void ratio was subsequently adopted as the independent variable to characterize the pore-structure dependence of the saturation-dependent coefficients. Because only four void-ratio levels were available, simple functional forms containing no more than two adjustable coefficients were considered to reduce the risk of overfitting. The initial functional forms were selected according to the variation trends obtained from Table 4.

The corresponding coefficients were then jointly calibrated against the complete experimental dataset under the constraints $a>0$, $b>0$, and $c>0$ within the investigated state range, thereby improving the numerical stability of the coupled formulation. The resulting constrained parameterization is presented in Table 5.

Table 5. Constrained parameterization of the saturation-dependent coefficients with respect to void ratio.

Pressure-model parameter	Saturation-dependent relationship	Coefficient	Calibrated relationship or value
a	$a=A_a+B_a\cdot S_r$	A_a	$A_a=-0.0464-0.278\ln(e)$
a	$a=A_a+B_a\cdot S_r$	B_a	$B_a=-2.89+3.47e$
b	$b=A_b+B_b\cdot S_r$	A_b	$A_b=0$
b	$b=A_b+B_b\cdot S_r$	B_b	$B_b=-7.67+10.1e$
c	$c=A_c+B_c\cdot \ln(S_r)$	A_c	$A_c=-0.0164-0.0838\ln(e)$
c	$c=A_c+B_c\cdot \ln(S_r)$	B_c	$B_c=0.0589-0.126e$

As shown in Table 5, the saturation-dependent coefficients were parameterized using simple functions of void ratio while preserving the functional structures identified from Table 4. Logarithmic relationships with e were adopted for A_a and A_c, whereas linear relationships were used for B_a, B_b, and B_c. During the constrained calibration, A_b was set to zero, allowing parameter b to be expressed directly through the saturation-dependent term B_bS_r. This simplification avoids introducing an additional weakly supported coefficient relationship and contributes to the numerical stability of the coupled formulation.

The coefficients listed in Table 5 were jointly calibrated against the complete experimental dataset under the constraints $a>0$, $b>0$, and $c>0$ within the investigated state range. These constraints ensure positive model parameters and prevent numerical divergence of the pressure-dependent response at high pressure. Because the coefficients were obtained through constrained joint calibration rather than independent regressions, the parameterization is evaluated based on the predictive performance of the complete three-factor coupled collapse-coefficient model rather than on the coefficients of determination of individual intermediate relationships.

Based on the functional structures identified in Table 4 and the constrained coefficient parameterization presented in Table 5, the pressure-model parameters can be expressed as continuous functions of S_r and e. Together with the fixed pressure exponents m=1.6 and n=1.0, these relationships define the final coupled formulation.

Accordingly, parameter a can be expressed as:

$$a(S_r,e)=\left[-0.0464-0.278ln(e)\right]+\left(-2.89+3.47e\right)S_r \quad (11)$$

Similarly, parameter b is given by:

$$b(Sr,e)=\left(-7.67+10.1e\right)S_r \quad (12)$$

Parameter c is expressed as:

$$c(Sr,e)=\left[-0.0164-0.0838ln(e)\right]+\left(0.0589-0.126e\right)ln(S_r) \quad (13)$$

where S_r is the degree of saturation expressed in decimal form and e is the void ratio. Because logarithmic terms are included in Eqs. (11) and (13), both S_r and e must be greater than zero. More importantly, these empirical relationships should be applied only within the experimentally investigated ranges of S_r and e.

Substituting Eqs. (11)–(13) into the pressure-dependent relationship yields the final three-factor coupled collapse-coefficient model:

$$\delta_s(P,S_r,e)=\left[a(S_r,e)P^{1.6}-c(S_r,e)\right]exp\left[-b(S_r,e)P\right]+c(S_r,e) \quad (14)$$

Within the proposed model, the dimensionless pressure P represents the normalized applied vertical pressure and describes the pressure-dependent evolution of the collapse

coefficient. The degree of saturation S_r characterizes the moisture state and the extent of pore-water filling and affects the magnitude and pressure-dependent evolution of the collapse response through parameters a, b, and c.The void ratio e characterizes the pore-structure state and accounts for the influence of soil density on the saturation-dependent parameter relationships. These three state variables do not contribute through independent additive terms; rather, their coupled effects are incorporated into the pressure-dependent collapse response through the model parameters.

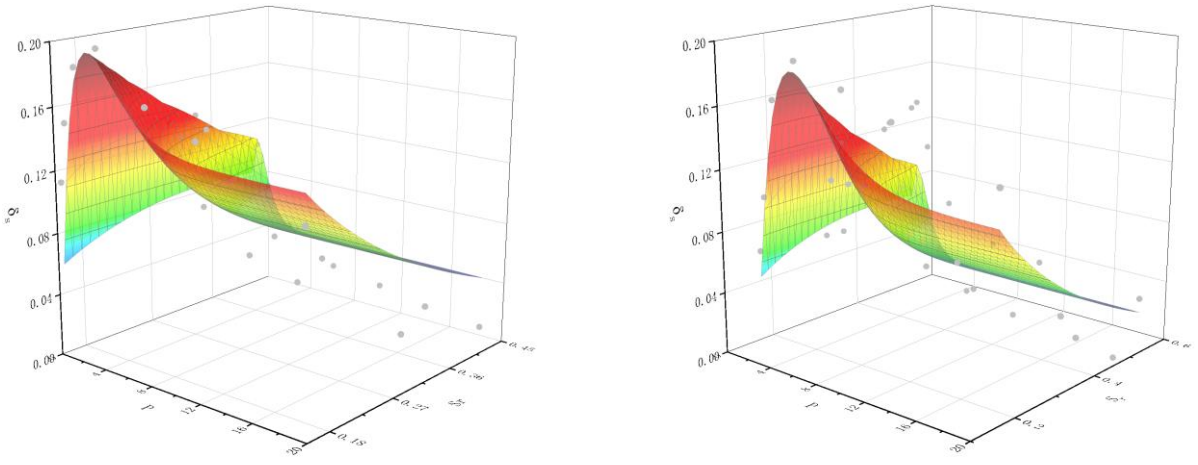
Although P, S_r, and e are the direct state variables used in Eq. (14), they are derived from experimentally controlled quantities, including applied vertical pressure, water content, and dry density. The proposed model therefore incorporates the coupled effects of applied vertical pressure, moisture state, and pore-structure state on the collapse coefficient. Compared with empirical relationships expressed directly in terms of water content or dry density, the use of degree of saturation and void ratio provides a more physically representative description of the soil state, particularly when specimens with the same water content exhibit different pore-structure states and degrees of pore-water filling.

Equation (14) was evaluated against all valid experimental data within the investigated ranges of applied vertical pressure, degree of saturation, and void ratio. The proposed three-factor coupled model yielded an overall coefficient of determination of R^2=0.783, with a root mean square error of 0.0217 and a mean absolute error of 0.0171. Overall, the model captured the principal variations in the collapse coefficient with applied vertical pressure, degree of saturation, and void ratio, although deviations remained under individual state conditions. These deviations may be associated with experimental scatter and the cumulative uncertainty introduced during the multistage parameterization and constrained-calibration procedure.

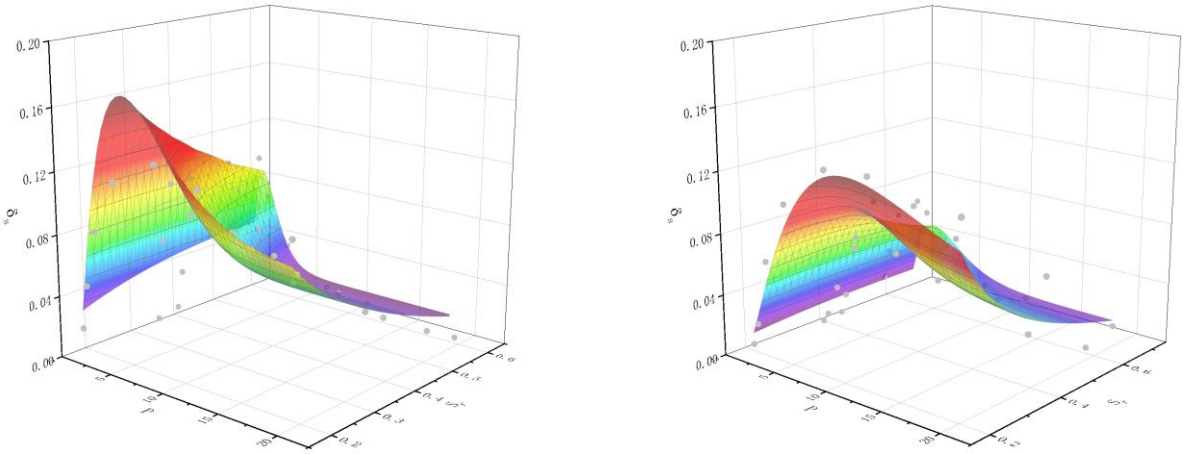
It should be emphasized that Eqs. (11)–(14) constitute an empirical formulation calibrated using remolded loess collected from the Ili region of Xinjiang, China. Therefore, the fitted coefficients are soil-specific and are primarily applicable to the tested Ili loess within the investigated ranges of applied vertical pressure, degree of saturation, and void ratio. In the present study, the applicable ranges are $50 \le p \le 2000$ kPa, $0.150 \le S_r \le 0.672$, and $0.850 \le e \le 1.194$. Application of the proposed model to loess from other regions or to soil states outside these ranges requires additional experimental calibration and validation.

For each void-ratio condition, the applicable range of S_r should be restricted to the corresponding experimentally measured range.

4.2 Model Validation



(**a**) (**b**)



(**c**) (**d**)

Figure 7. Comparison between the model-predicted response surfaces and measured collapse coefficients under different void-ratio conditions: (**a**) *e*=1.194; (**b**) *e*=1.0763; (**c**) *e*=0.957; (**d**) *e*=0.85.

Figure 7 compares the model-predicted response surfaces with the measured data under different void-ratio conditions. Overall, the model adequately reproduces the principal variations in the collapse coefficient with dimensionless pressure and degree of saturation.

At a given void ratio, the collapse coefficient generally increased with dimensionless pressure over the low-pressure range, reached a peak within an intermediate pressure range, and then gradually decreased. At the same time, the collapse coefficient showed an overall decreasing trend with increasing degree of saturation. Both the peak magnitude and the pressure corresponding to the peak varied among the different void-ratio conditions, indicating that the pore-structure state influenced both the magnitude and pressure-dependent evolution of the collapse response.

The measured data generally followed the overall trends represented by the model-predicted surfaces, although noticeable deviations remained under some state conditions. These results indicate that, within the investigated range, the proposed three-factor coupled model can reasonably characterize the combined effects of dimensionless pressure, degree of saturation, and void ratio.

4.3 Model Application Procedure

Once e and Sr have been determined, the applied vertical pressure p is normalized using Eq. (1) to obtain the dimensionless pressure P. The void ratio e is then substituted into the constrained parameterization presented in Table 5 to determine A_a, B_a, A_b, B_b, A_c, and B_c. These coefficients, together with the degree of saturation, are subsequently substituted into Eqs. (11)–(13) to obtain the corresponding values of a, b, and c.

Finally, the resulting parameter values and the dimensionless pressure P are substituted into Eq. (14) to determine the collapse coefficient δ_s for the specified soil state. The calculated value can then be compared with the criterion of δ_s=0.015. A soil state is classified as collapsible when $\delta_s \geq 0.015$, whereas $\delta_s < 0.015$ indicates a non-collapsible state under the specified condition.

The proposed model can be applied not only to individual-state calculations but also to continuous parametric analyses. At fixed void ratio and degree of saturation, varying the dimensionless pressure generates the corresponding pressure–collapse coefficient curve. At fixed void ratio, simultaneous variation in dimensionless pressure and degree of saturation produces a three-dimensional response surface. The degree of saturation may also be varied according to the moisture-induced evaluation framework established in Section 4.5 to examine changes in collapse potential during progressive wetting. The

model can therefore be readily implemented for batch calculations and systematic parametric analyses.

The overall back-calculation results indicate that the proposed model captures the principal variations in the collapse coefficient with dimensionless pressure, degree of saturation, and void ratio. Nevertheless, discrepancies remain between the calculated and measured values under certain conditions. These deviations may result from experimental scatter, uncertainties in the intermediate parameter relationships, and the multistage parameterization and constrained-calibration procedure. Therefore, the proposed formulation should be regarded as an empirical prediction model applicable within the investigated state range rather than as a universal relationship independent of soil type and soil state. The present model does not explicitly account for differences in soil fabric, mineralogical composition, or other soil-specific characteristics. Therefore, additional calibration and validation are required before the model is applied to loess from other regions or to soil states substantially different from those investigated in this study.

Overall, the proposed model integrates the effects of moisture state, pore-structure state, and applied vertical pressure into a unified continuous formulation. Within the investigated state range, the model enables direct calculation of the collapse coefficient for a specified soil state and evaluation of changes in the remaining collapse potential during progressive wetting.

4.4 Engineering-Scale Evaluation Using a Field Immersion Test

To further examine the engineering applicability of the proposed three-factor coupled collapse-coefficient model, a large-scale field immersion test of Ili loess reported by Zhang et al. [29] was selected for comparison. The test was conducted at a large channel project in the Ili region of Xinjiang, China, where an approximately 30-m-thick collapsible loess deposit was investigated. Zhang et al. [29] reported the depth-dependent distributions of natural water content and dry density and obtained a measured self-weight collapse of 3520 mm from the field immersion test. These field data provide an engineering-scale basis for evaluating whether the proposed model can estimate foundation self-weight collapse from routinely obtainable soil-state parameters.

The 30 m loess profile was discretized into 30 soil layers, each with a thickness of 1 m. The representative calculation depth of each layer was taken at its midpoint. Therefore, the calculation depths were 0.5, 1.5, 2.5, …, and 29.5 m. The measured natural water content and dry density corresponding to each depth interval were adopted as the representative soil-state parameters of the corresponding layer.

For each soil layer, the void ratio e_i and degree of saturation $S_{r,i}$ were calculated from the corresponding dry density and natural water content using Eqs. (2) and (3), respectively.

Because the collapse response of each 1 m layer was evaluated at the midpoint of the layer, the representative self-weight vertical pressure was calculated as the mean of the pressures at the upper and lower boundaries:

$$p_{m,i} = \frac{p_{i-1} + p_i}{2} \tag{20}$$

where p_i and p_{i-1} are the accumulated self-weight vertical pressures at the lower and upper boundaries of the ith layer, respectively, and p_0=0.

The self-weight vertical pressure at the midpoint of each layer was then normalized by the reference atmospheric pressure:

$$p_i = \frac{p_{m,i}}{101.3} \tag{21}$$

The resulting P_i, $S_{r,i}$, and e_i were substituted into Eqs. (11)–(14) to calculate the model-predicted collapse coefficient $\delta_{zs,i}$ corresponding to the self-weight pressure at the mid-point of the ith soil layer.The self-weight collapse contribution of each layer was subsequently calculated as

$$\Delta s_{zs,i} = \delta_{zs,i} h_i \quad (22)$$

where h_i=1000 mm is the thickness of the ith soil layer. Following the collapse criterion adopted in this study, layers with $\delta_{zs,i}$<0.015 were excluded from the accumulation. Therefore, the total model-predicted self-weight collapse was calculated as

$$\Delta_{zs,model} = \sum_{i=1}^{n} \delta_{zs,i} h_i, \delta_{zs,i} \geq 0.015 \quad (23)$$

The above procedure was applied successively to all 30 soil layers. For example, the representative self-weight pressures at depths of 0.5, 1.5, and 2.5 m were 8.90, 26.75, and 44.55 kPa, respectively. The corresponding soil-state parameters were substituted into Eqs. (11)–(14) to determine the model-predicted collapse coefficient of each layer. The predicted collapse coefficient of the shallowest 0–1 m layer was 0.0105, which was lower than the collapse criterion of 0.015 and was therefore excluded from the accumulation of self-weight collapse. The remaining 29 layers exhibited predicted collapse coefficients greater than 0.015 and were included in the calculation.

Summation of the collapse deformation of the layers satisfying the collapse criterion yielded a total model-predicted self-weight collapse of

$$\Delta_{zs,model} = 3330.71 mm.$$

The corresponding self-weight collapse measured in the large-scale field immersion test reported by Zhang et al. [29] was

$$\Delta_{zs,field} = 3520 mm.$$

The proposed model therefore underestimated the field-measured self-weight collapse by 189.29 mm, corresponding to a relative error of 5.38%. Considering the spatial variability of natural loess and the fact that the model parameters were calibrated using laboratory remolded specimens, the calculated result shows reasonably good agreement with the field measurement. The engineering-scale comparison indicates that the proposed coupled formulation can reasonably estimate the overall magnitude of self-weight collapse using depth-dependent soil-state parameters and self-weight pressure.

The calculation also demonstrates the practical application procedure of the proposed model. Once the vertical distributions of water content and dry density of a loess foundation are available, the corresponding void ratio and degree of saturation can be determined for each soil layer. Combined with the self-weight vertical pressure at the representative depth of each layer, Eqs. (11)–(14) can be used to calculate the depth-dependent collapse coefficient and subsequently estimate the total self-weight collapse of the foundation. Therefore, the proposed formulation establishes a direct quantitative link between routinely measurable soil properties and foundation-scale self-weight collapse and provides a potential basis for engineering assessment of collapsible loess foundations.

It should be noted that several field calculation points extend slightly beyond the state ranges used for laboratory model calibration. In particular, the representative self-weight pressures of the first three layers are lower than the minimum laboratory pressure of 50 kPa, while several loose soil layers exhibit void ratios greater than the calibrated upper limit of e=1.194.. Therefore, although the calculated self-weight collapse agrees reasonably well with the field measurement, the present comparison should be regarded as an engineering-scale application of the proposed model. Additional laboratory and field data covering broader stress and pore-structure conditions are required to further evaluate its general applicability.

4.5 Moisture-Induced Evaluation Framework

The three-factor coupled model established in Section 4.1 expresses the collapse coefficient as a continuous function of dimensionless pressure, degree of saturation, and void ratio. In engineering environments involving water infiltration, loess foundations typically experience progressive wetting rather than instantaneous saturation. Reservoir impoundment, groundwater rise, prolonged rainfall infiltration, and leakage from water-conveyance structures can progressively alter the soil moisture state. Therefore, evaluating collapsibility solely on the basis of the initial moisture state cannot fully capture the evolution of collapse potential during continued wetting.

To extend the model from discrete moisture states to progressive wetting conditions, a dimensionless wetting parameter, S_w, is introduced to quantify the relative progression of wetting from the initial moisture state toward the theoretical saturated state.

$$S_w = \frac{w_I - w_0}{w_{sat} - w_0} \tag{24}$$

where S_w denotes the dimensionless wetting parameter, w_0 is the initial water content, w_i is the water content corresponding to a given wetting stage, and w_{sat} is the theoretical saturated water content. All water-content values are expressed in decimal form in the calculations.

When S_w=0, the soil remains at its initial moisture state, whereas S_w increases progressively as wetting proceeds. Theoretically, S_w=1 corresponds to the saturated state. Therefore, S_w provides a normalized measure of wetting progression from the initial moisture state toward the theoretical saturated state.

For a given void ratio, the saturated state corresponds to S_r=1. Accordingly, the theoretical saturated water content can be expressed as:

$$w_{sat} = \frac{e}{G_s} \tag{25}$$

where e is the void ratio and G_s is the specific gravity of the soil solids.

Combining the above expression with the degree-of-saturation relationship given in Eq. (3) yields the following relationship between the wetting parameter and the degree of saturation:

$$S_r = S_{r0} + S_\omega\left(1 - S_{r0}\right) \tag{26}$$

where S_{r0} denotes the initial degree of saturation.Equation (26) shows that, for a fixed void ratio, the degree of saturation S_r increases linearly with the wetting parameter S_w. This relationship provides a direct link between the progressive-wetting framework and the three-factor coupled model established in Section 4.1.

At a given wetting stage, S_w and S_r are first determined from the corresponding water content.using Eqs. (24) and (26). The resulting S_r,together with P and e, is then substituted into Eq. (14) to calculate the collapse coefficient at the corresponding wetting stage.

In this study, the lowest tested water content of 6.6% was taken as the initial state of the representative wetting path, while the tested water contents of 12.5%, 14.1%, 18.2%, and 21.0% were regarded as successive wetting stages. The corresponding ranges of the wetting parameter and degree of saturation under different dry-density conditions are summarized in Table 6.

Table 6. Ranges of wetting parameter and degree of saturation under different dry-density conditions.

ρ_d/(g/cm³)	e	w_{sat}(%)	Measured water-content range	S_w	S_r=0.5
1.24	1.194	43.88	6.6-18.2	0–0.31	0.15–0.41

ρ_d/(g/cm³)	e	w_{sat}(%)	Measured water-content range	S_w	S_r=0.5
1.31	1.076	39.57	6.6-21.0	0–0.44	0.17–0.53
1.39	0.957	35.18	6.6-21.0	0–0.50	0.19–0.60
1.47	0.850	31.26	6.6-21.0	0–0.58	0.21–0.67

As shown in Table 6, the maximum wetting parameter covered by the experiments was 0.584, and the maximum degree of saturation was 0.672, indicating that the saturated state was not reached. Therefore, the subsequent wetting analysis is restricted to the experimentally investigated range, and no extrapolation to $S_w = 1.0$ is performed.

It should be noted that the different water-content states investigated in this study were obtained from separately prepared specimens rather than through continuous wetting of the same specimen. Accordingly, the representative wetting sequence established herein was reconstructed from independently prepared specimens at discrete moisture states and is intended to characterize the overall evolution of collapse potential during progressive wetting.

4.6 Variation in the Collapse Coefficient during Progressive Wetting

After determining the water content and degree of saturation corresponding to each wetting stage, the dimensionless pressure P, degree of saturation Sr, and void ratio e were substituted into the three-factor coupled model to calculate the collapse coefficient at each wetting state. All valid data within the experimentally investigated range were included in the subsequent analysis. For an increase in the wetting parameter from S_{w1} to S_{w2}, the reduction in the collapse coefficient during that stage was calculated as follows:

$$\Delta\delta_s^{S_{w1}\to S_{w2}} = \overline{\delta_s}(S_{w1}) - \overline{\delta_s}(S_{w2}) \tag{27}$$

where $\delta_s(S_{w1})$ and $\delta_s(S_{w2})$ are the mean collapse coefficients corresponding to two successive wetting states. $\Delta\delta_s$ represents the reduction in the collapse coefficient between two successive wetting states and is used as an indicator of the reduction in the remaining collapse potential during the corresponding wetting stage.

To examine the overall saturation-dependent variation in collapse potential and evaluate whether the proposed model captures this trend, the measured and calculated results were grouped according to the experimentally covered degree-of-saturation range.

The measured degree of saturation ranged from 0.15 to 0.672. Based on the distribution of the data, this range was divided into four intervals: 0.15–0.30, 0.30–0.40, 0.40–0.50, and 0.50–0.672. Here, a degree-of-saturation interval refers to a specified range of S_r used to group the measured and model-calculated results for statistical comparison.The mean measured and model-calculated collapse coefficients were then determined for each interval.

To further compare the relative distribution of the collapse coefficient among different saturation intervals, the mean collapse coefficient in each interval was normalized by the sum of the mean values over all four intervals. The normalized proportion for the ith saturation interval was calculated as follows:

$$\eta_i = \frac{\delta_{si}}{\sum \delta_{sj}} \times 100\% \tag{28}$$

where η_i is the normalized proportion of the mean collapse coefficient in the ith saturation interval, δ_s,i is the corresponding mean collapse coefficient, and the denominator represents the sum of the mean collapse coefficients over all four saturation intervals.

Table 7. Comparison of mean measured and model-calculated collapse coefficients and their normalized proportions within different degree-of-saturation intervals.

Degree-of-saturation interval S_r	Mean measured collapse coefficient	Mean calculated collapse coefficient	Measured normalized proportion/%	Calculated normalized proportion%
0.15–0.30	0.111	0.108	39.16	37.82
0.30–0.40	0.0677	0.077	23.83	26.8
0.40–0.50	0.0551	0.060	19.38	21.05
0.5–0.672	0.0501	0.041	17.63	14.34

As shown in Table 7, both the measured and model-calculated mean collapse coefficients decreased continuously with increasing degree of saturation. The measured mean collapse coefficient decreased from 0.111 in the lowest saturation interval to 0.0501 in the highest saturation interval, while the corresponding model-calculated value decreased from 0.108 to 0.041. This consistent overall trend indicates that increasing degree of saturation was associated with a progressive reduction in the remaining collapse potentialt.

According to Eq. (24), the reductions in the measured mean collapse coefficient between the three pairs of adjacent saturation intervals were 0.0433, 0.0126, and 0.005, respectively. The progressively smaller reductions indicate that the decrease in the interval-averaged remaining collapse potential became less pronounced at higher degrees of saturation. For comparison, the corresponding reductions obtained from the model-calculated mean collapse coefficients were 0.031, 0.017, and 0.019, respectively. Although the model-calculated reductions did not exhibit the same progressively decreasing magnitude as the measured results, the model reproduced the overall decrease in the mean collapse coefficient with increasing degree of saturation.

Within the highest saturation interval (Sr=0.500–0.672), the measured normalized proportion decreased to 17.63%, whereas the model-calculated value was 14.34%, corresponding to a difference of 3.29 percentage points. Together with the overall decrease in the interval-averaged collapse coefficients, these results indicate that the relative contribution of higher degree-of-saturation states to the overall collapse response was comparatively smaller. The proposed model captured this overall redistribution reasonably well, although it moderately underestimated the relative response within the highest saturation interval.

5 Conclusions

(1) The collapse coefficient of remolded Ili loess was jointly influenced by moisture state, pore-structure state, and applied vertical pressure. The collapse coefficient generally decreased with increasing water content and degree of saturation, while the influence of void ratio varied with moisture state and applied pressure. The pressure-dependent response was distinctly nonlinear, generally exhibiting an initial increase, a peak within an intermediate pressure range, and a subsequent decrease. These results indicate that the collapse response cannot be adequately characterized by a single state variable.

(2) A three-factor coupled collapse-coefficient model was developed using dimensionless pressure P, degree of saturation S_r, and void ratio e as the governing state variables. With the pressure exponents fixed at m=1.6 and n=1.0, the saturation- and void-ratio-dependent parameter relationships were established through constrained parameterization. Back-calculation using all experimental data points yielded an overall coefficient of determination of R^2=0.783, with RMSE = 0.0217 and MAE = 0.0171. The results indicate that the model captures the principal variations in the collapse coefficient within the investigated state range.

(3) The collapse response showed an overall reduction with increasing degree of saturation. Across the four degree-of-saturation intervals of 0.150–0.300, 0.300–0.400, 0.400–0.500, and 0.500–0.672, the measured normalized proportions of the interval-averaged collapse coefficients were 39.16%, 23.83%, 19.38%, and 17.63%, respectively, while the corresponding model-calculated proportions were 37.82%, 26.80%, 21.05%, and 14.34%. The

model reproduced the overall decreasing distribution with increasing degree of saturation, although some discrepancy remained in the highest saturation interval. The moisture-induced evaluation framework therefore provides a quantitative means of characterizing changes in the remaining collapse potential with increasing moisture state.

(4) The engineering applicability of the proposed formulation was further examined using a large-scale field immersion test conducted in the Ili region. Based on the reported 30 m soil profile, the foundation was discretized into 1 m layers, and the self-weight pressure at the midpoint of each layer was combined with the corresponding moisture and pore-structure states to calculate the layer wise collapse response. The proposed model predicted a total self-weight collapse of 3330.71 mm, compared with the field-measured value of 3520 mm, corresponding to a relative error of 5.38%. This engineering-scale comparison demonstrates the potential of the proposed formulation for estimating foundation self-weight collapse from depth-dependent water-content and dry-density data.

(5) The proposed formulation is an empirical model calibrated using remolded Ili loess and is primarily applicable within the experimentally investigated ranges of $50 \le p \le 2000$ kPa, $0.150 \le S_r \le 0.672$, and $0.850 \le e \le 1.194$. Several shallow field calculation points in the engineering application extended slightly beyond these calibration ranges; therefore, the field comparison should be interpreted as an engineering-scale application rather than strict independent validation. Further laboratory and field calibration is required before the model is applied to loess from other regions or to substantially different stress, moisture, and pore-structure conditions.

Funding: This work was supported by the Youth Project of the Shaanxi Provincial Department of Science and Technology (Grant No. 2026JC-YBQN-0452).

Data Availability:The laboratory data generated and analyzed during the current study are included in the Supplementary Information accompanying this article.

References

1. Yu BW, Liu GH, Liu QS, Huang C, Li H, Zhao ZH. "Seasonal variation of deep soil moisture under different land uses on the semi-arid Loess Plateau of China." Journal of Soils and Sediments, vol. 19, no. 3, pp. 1179–1189, 2019.
2. Feng SJ, Du FL, Shi ZM, Shui WH, Tan K. "Field study on the reinforcement of collapsible loess using dynamic compaction." Engineering Geology, vol. 185, pp. 105–115, 2015.
3. Luo H, Wu FQ, Chang JY, Xu J. "Microstructural constraints on geotechnical properties of Malan loess: A case study from Zhaojiaan landslide in Shaanxi Province, China." Engineering Geology, vol. 236, pp. 60–69, 2018.
4. Zhang YW, Song ZP, Chen HC, Ruan L, He SM. "Experimental study on collapsible and structural characteristics of artificially prepared loess material." Scientific Reports, vol. 13, article 4113, 2023.
5. Li P, Vanapalli SK, Li TL. "Review of collapse triggering mechanism of collapsible soils due to wetting." Journal of Rock Mechanics and Geotechnical Engineering, vol. 8, no. 2, pp. 256–274, 2016.
6. Jiang MJ, Zhang FG, Hu HJ, Cui YJ, Peng JB. "Structural characterization of natural loess and remolded loess under triaxial tests." Engineering Geology, vol. 181, pp. 249–260, 2014.
7. Zhang YW, Song ZP, Weng XL. "A constitutive model for loess considering the characteristics of structurality and anisotropy." Soil Mechanics and Foundation Engineering, vol. 59, no. 1, pp. 32–43, 2022.
8. Wang L, Li XA, Li LC, Hong B, Yao W, Lei HN, et al. "Characterization of the collapsible mechanisms of Malan loess on the Chinese Loess Plateau and their effects on eroded loess landforms." Human and Ecological Risk Assessment: An International Journal, vol. 26, no. 9, pp. 2541–2566, 2020.
9. Xie WL, Li P, Vanapalli SK, Wang JD. "Prediction of the wetting-induced collapse behaviour using the soil–water characteristic curve." Journal of Asian Earth Sciences, vol. 151, pp. 259–268, 2018.
10. Wang JD, Li P, Ma Y, Vanapalli SK, Wang XG. "Change in pore-size distribution of collapsible loess due to loading and inundating." Acta Geotechnica, vol. 15, no. 5, pp. 1081–1094, 2020.
11. Xu L, Gao C, Lan T, Lei J, Zuo L. "Influence of grading on the compressibility of saturated loess soils." Géotechnique Letters, vol. 10, no. 2, pp. 198–204, 2020.
12. Shao SJ, Wang LQ, Shao S, Wang Q. "Structural yield and collapse deformation of loess." Chinese Journal of Geotechnical Engineering, vol. 39, no. 8, pp. 1357–1365, 2017. (in Chinese).

13. Liu Y, Zhao Y, Zhang J, Uge BU, Du Z, Nie W. "Load transfer mechanism variations of bored piles in collapsible loess subjected to water infiltration." Journal of Geotechnical and Geoenvironmental Engineering, vol. 151, no. 4, article 04025008, 2025.
14. Yang YS, Li J, Xing YC, Zhao JM. "Experimental study on moistening deformation characteristics of compacted loess and their influencing factors." Chinese Journal of Geotechnical Engineering, vol. 39, no. 4, pp. 626–635, 2017. (in Chinese).
15. Xu P, Miao HC, Shao SJ, Fang LY. "Research on wetting and collapsible deformation characteristics of collapsible loess under different triaxial stress conditions." Chinese Journal of Applied Mechanics, vol. 38, no. 5, pp. 1966–1973, 2021. (in Chinese).
16. Shao SJ, Li J, Li GL, Wang XD, Jin BC, Shao S. "Field immersion tests on tunnel in large-thickness collapsible loess." Chinese Journal of Geotechnical Engineering, vol. 40, no. 8, pp. 1395–1404, 2018. (in Chinese). https://doi.org/10.11779/CJGE201808004
17. Wu XP, Wang LM, Fang JH, Xu AH, Zhou YL, Zhao YH. "Seepage characteristics and their relationship with self-weight collapse of intact loess ground." Chinese Journal of Geotechnical Engineering, vol. 40, no. 6, pp. 1002–1010, 2018. (in Chinese).
18. Zhang DF, Chen CL, Chen H, Liu K. "Wetting permeability of intact loess under triaxial stress conditions." Chinese Journal of Geotechnical Engineering, vol. 40, no. S1, pp. 45–50, 2018. (in Chinese).
19. Di SJ, Zhang Y, Zhou H, Xie WL, He XL, Li YT, Mu QY. "Effects of compaction water content on water retention and deformation behavior of compacted loess." Advances in Civil Engineering, vol. 2024, article 5510839, 2024.
20. Wang YY, Li YR. "Wetting-induced collapse of loess: Tracing microstructural evolution." Engineering Geology, vol. 340, article 107673, 2024.
21. Zhuang JQ, Kong JX, Zhu Y, Peng JB. "The structural evolution of undisturbed loess due to water infiltration." Scientific Reports, vol. 14, article 14880, 2024.
22. Liang ZC, Zhang AJ, Ren WY, Hu HJ, Wang YG. "Investigating the curing time effect on water retention property and microstructure of lime-treated Ili loess." Bulletin of Engineering Geology and the Environment, vol. 82, no. 7, article 241, 2023.
23. Ministry of Housing and Urban-Rural Development of the People's Republic of China. Standard for Geotechnical Testing Method: GB/T 50123–2019. China Planning Press, Beijing, China, 2019. (in Chinese).
24. Ministry of Housing and Urban-Rural Development of the People's Republic of China. Standard for Building Construction in Collapsible Loess Regions: GB 50025–2018. China Architecture & Building Press, Beijing, China, 2018. (in Chinese).
25. Liang ZC, Ren WY, Li SC, Zhang AJ, Wang YG, Niu LS, Hu HJ. "Impact of soluble salt content on unfrozen water and matric suction during cooling of loess in Ili region, China." Bulletin of Engineering Geology and the Environment, vol. 84, no. 3, article 117, 2025.
26. Sun XH, Li X, Li M, Luo YS, Wang JL, Yin ZM, Hu HJ. "Study on the compression and collapsibility characteristics of Yangling loess under different wet and dense states." Applied Sciences, vol. 15, no. 24, article 12879, 2025.
27. Marei MG, Abdelaziz TM, Ragheb AM, Ali N. "A proposed approach for calculating collapse settlement." In Novel Issues on Unsaturated Soil Mechanics and Rock Engineering, Springer, Cham, Switzerland, pp. 82–96, 2019.
28. Wang LQ, Lu ZG, Shao SJ. "New nonlinear stress-strain model for loess and its comparative research." Chinese Journal of Geotechnical Engineering, vol. 39, no. 9, pp. 1724–1730, 2017. (in Chinese).
29. Zhang AJ, Xing YC, Hu XL, Wang HT, Guo MX, Zhang B, Gao YP. "Influence factors of strong self-weight collapsibility of Ili loess." Chinese Journal of Geotechnical Engineering, vol. 38, no. S2, pp. 117–122, 2016. (in Chinese).

Supplementary Files

This is a list of supplementary files associated with this preprint. Click to download.

- SupplementaryData.xlsx